MADRID
inter.noise 2019
June 16 - 19
NOISE CONTROL FOR A BETTER ENVIRONMENT

Beamforming by Means of Inverse Variance Weighting

Raumer, Hans-Georg[1]
German Aerospace Center (DLR)
Bunsenstr. 10, 37073 Göttingen

ABSTRACT

Conventional beamforming is one of the standard methods for localization and quantification of aeroacoustic sources in wind tunnel testing. It offers a robust indicator for the sound source distribution. The conventional beamformer minimizes the deviation between the synthetic and measured cross correlation matrix with respect to the Frobenius norm. This approach imposes the assumption that the measured cross correlations are superposed with uncorrelated white noise. In real-life applications this idealized noise model is often violated. We consider a slightly relaxed noise model where the noise is still uncorrelated but non-white. Assuming non-white noise we end up with a modified beamformer that minimizes the deviation with respect to a weighted Frobenius norm. The application of this approach on experimental data of a wind tunnel test shows that the resolution and dynamic range of the source maps can be enhanced compared to conventional beamforming.

Keywords: Array imaging, Beamforming, Aeroacoustics
I-INCE Classification of Subject Number: 74, 76, 77

1. INTRODUCTION

Beamforming methods are well established for the treatment of aeroacoustic source problems like jet noise [1] or model testing in closed wind tunnels [2]. They offer a fast and robust way to obtain an estimator of the source power distribution of aeroacoustic sources.

For a discrete set of microphones/sensors at positions $\{\mathbf{x}_1, \ldots, \mathbf{x}_M\}$ we record sound pressure signals $p(\mathbf{x}_m, t)$. Since the pressure signal is a stochastic quantity we can only estimate the cross correlation of each sensor pairing. This process is usually done in the frequency domain and yields the *Cross Spectral Matrix* (CSM) with entries

$$\mathbf{C}_{ml}(\omega) = \mathbb{E}\left[\hat{p}(\mathbf{x}_m, \omega)\hat{p}(\mathbf{x}_l, \omega)^*\right] \qquad m, l = 1, \ldots, M\ . \tag{1}$$

[1]hans-georg.raumer@dlr.de

The hat denotes the Fourier transform of the sound signal, ω is the angular frequency and the star denotes the complex conjugation. In practice the expectation operator is carried out by sample averaging.

Given the array data (cross correlations in our case) we aim to localize and quantify the sound power of the unknown source term in a region of interest $\mathcal{Y} \subset \mathbb{R}^3$. For each focus point $\mathbf{y} \in \mathcal{Y}$ an estimator of the source power is computed independently of the other focus points.

2. BEAMFORMING METHODS

2.1 Sound Propagation

Neglecting the geometry of the wind tunnel test section and assuming a constant flow field $\mathbf{u} = (u_1, u_2, u_3)^T$ the sound propagation in frequency domain is modelled by the free field convective Helmholtz equation

$$k^2\hat{p} + 2ik\sum_{j=1}^{3}\frac{u_j}{c}\frac{\partial\hat{p}}{\partial x_j} + \sum_{j=1}^{3}\left(\left(\frac{u_j}{c}\right)^2 - 1\right)\frac{\partial^2\hat{p}}{\partial x_j^2} = -q\,, \tag{2}$$

with a source term q, the speed of sound c and wavenumber $k = \frac{\omega}{c}$. The Green's function $g(\mathbf{x}, \mathbf{y}, \omega)$ is the solution of Equation 2 with a Dirac source term at position $\mathbf{y}$ i.e. $q = \delta(\mathbf{x} - \mathbf{y})$. Using the Mach vector $\mathbf{v} = \frac{1}{c}\mathbf{u}$ the Green's function reads as

$$g(\mathbf{x}, \mathbf{y}, \omega) = \frac{\exp\left(-ik\,\frac{(\mathbf{y}-\mathbf{x})\cdot\mathbf{v} + \sqrt{((\mathbf{x}-\mathbf{y})\cdot\mathbf{v})^2 + (1-\|\mathbf{v}\|_2^2)\|\mathbf{x}-\mathbf{y}\|_2^2}}{1-\|\mathbf{v}\|_2^2}\right)}{4\pi\sqrt{((\mathbf{x}-\mathbf{y})\cdot\mathbf{v})^2 + (1-\|\mathbf{v}\|_2^2)\|\mathbf{x}-\mathbf{y}\|_2^2}}\,. \tag{3}$$

For any $\mathbf{y} \in \mathcal{Y}$ we define the *steering vector*

$$\mathbf{g}(\mathbf{y}, \omega) = \begin{pmatrix} g(\mathbf{x}_1, \mathbf{y}, \omega) \\ \vdots \\ g(\mathbf{x}_M, \mathbf{y}, \omega) \end{pmatrix} \in \mathbb{C}^M \tag{4}$$

and the corresponding *steering matrix*

$$\mathbf{G}(\mathbf{y}, \omega) = \mathbf{g}(\mathbf{y}, \omega)\mathbf{g}(\mathbf{y}, \omega)^*\,. \tag{5}$$

2.2 Conventional Beamforming

We will start our investigation of the beamforming process with its characterization as a minimization problem according to Sijtsma [3] and adapt the notation of this reference.
Let $S \subset \{1, \ldots, M\}^2$ be a symmetric subset of index pairs, which indicates the correlation measurements that are taken into account for the imaging method. We set $\mathbf{C}_{ml}$ and $\mathbf{G}_{ml}$ to zero for $(m, l) \notin S$. Again, the resulting matricies will be denoted by $\mathbf{C}$ resp. $\mathbf{G}$. Often, we neglect autocorrelations of the microphones i.e. $S = \{(m, l) \in \{1, \ldots, M\}^2 : m \neq l\}$, because the noise level of the autocorrelation measurements is higher than the noise level of cross correlation measurements.

The conventional beamformer is defined as

$$B^{\mathrm{c}}(\mathbf{y},\omega) = \underset{\mu\in\mathbb{R}}{\operatorname{argmin}} \left\|\mathbf{C}-\mu\mathbf{G}\right\|_F^2 = \underset{\mu\in\mathbb{R}}{\operatorname{argmin}} \sum_{(m,l)\in S} \left|\mathbf{C}_{ml}-\mu\mathbf{G}_{ml}\right|^2 . \tag{6}$$

Explicitly solving Equation 6 yields the minimizer

$$B^{\mathrm{c}}(\mathbf{y},\omega) = Re\left(\frac{\langle\mathbf{C},\mathbf{G}\rangle_F}{\langle\mathbf{G},\mathbf{G}\rangle_F}\right) = Re\left(\frac{\sum\limits_{(m,l)\in S}\mathbf{C}_{ml}\mathbf{G}^*_{ml}}{\sum\limits_{(m,l)\in S}\left|\mathbf{G}_{ml}\right|^2}\right) \tag{7}$$

2.3 Inverse Variance Beamforming

As presented in Equation 1, the CSM can be considered as the expectation of a stochastic quantity. In the experiment we approximate this expectation value by a sample average. The conventional beamforming minimization problem (Equation 6) assumes that the mean square error is constant for all considered CSM entries i.e. $\exists\sigma^2 > 0$ s.t.

$$\mathbb{E}\left[\left|\hat{p}(\mathbf{x}_m,\omega)\hat{p}(\mathbf{x}_l,\omega)^* - \mathbf{C}_{ml}\right|^2\right] = \sigma^2 \quad \forall(m,l)\in S\,. \tag{8}$$

In the following we will relax this white noise model assumption and assume that the variances of the CSM entries may vary

$$\sigma^2_{ml} = \mathbb{E}\left[\left|\hat{p}(\mathbf{x}_m,\omega)\hat{p}(\mathbf{x}_l,\omega)^* - \mathbf{C}_{ml}\right|^2\right] \quad (m,l)\in S\,, \tag{9}$$

which corresponds to a noise model with uncorrelated but not necessarily white noise. The variance values σ^2_{ml} can be estimated by sample variances of the recorded data.

Any symmetric matrix $\mathbf{W}\in\mathbb{R}^{M\times M}$ with positive entries $\mathbf{W}_{ml} > 0\,, \forall m,l = 1,\ldots,M$ defines a scalar product on $\mathbb{C}^{M\times M}$ by

$$\langle\mathbf{A},\mathbf{B}\rangle_{\mathbf{W}} = \sum_{m,l=1}^{M}\mathbf{W}_{ml}\mathbf{A}_{ml}\mathbf{B}^*_{ml}\,, \tag{10}$$

with the induced norm

$$\|\mathbf{A}\|_{\mathbf{W}} = \sqrt{\sum_{m,l=1}^{M}\mathbf{W}_{ml}\left|\mathbf{A}_{ml}\right|^2}\,. \tag{11}$$

The idea of inverse variance beamforming is to solve the minimization problem in Equation 6 with respect to a weighted Frobenius norm with the following choice for the weighting matrix

$$\mathbf{W}_{ml} = \frac{1}{\sigma^2_{ml}}\,. \tag{12}$$

Hence we obtain the inverse variance beamformer by

$$B^{\mathrm{iv}}(\mathbf{y},\omega) = \underset{\mu\in\mathbb{R}}{\operatorname{argmin}} \left\|\mathbf{C}-\mu\mathbf{G}\right\|_{\mathbf{W}}^2 = \underset{\mu\in\mathbb{R}}{\operatorname{argmin}} \sum_{(m,l)\in S}\frac{1}{\sigma^2_{ml}}\left|\mathbf{C}_{ml}-\mu\mathbf{G}_{ml}\right|^2 . \tag{13}$$

Analogously to Equation 7 we find the minimizer

$$B^{\mathrm{iv}}(\mathbf{y},\omega) = Re\left(\frac{\langle \mathbf{C},\mathbf{G}\rangle_{\mathbf{W}}}{\langle \mathbf{G},\mathbf{G}\rangle_{\mathbf{W}}}\right) = Re\left(\frac{\sum\limits_{(m,l)\in S} \frac{1}{\sigma^2_{ml}}\mathbf{C}_{ml}\mathbf{G}^*_{ml}}{\sum\limits_{(m,l)\in S} \frac{1}{\sigma^2_{ml}}\left|\mathbf{G}_{ml}\right|^2}\right) . \tag{14}$$

The main additional effort of inverse variance beamforming compared to conventional beamforming is the computation of the sample variances. Once the variances of the cross correlations are stored, the computational effort increases only by a maximum factor of 2.

3. RESULTS

In this section we will investigate how the inverse variance weighting affects the beamforming result. The experimental wind tunnel data is taken from a benchmark measurement at the cryogenic wind tunnel in Cologne (DNW-KKK) [4], [5]. The benchmark test considers a scaled DO-728 half-model for different Mach numbers (0.15, 0.2, 0.25) and angles of attack (3°, 5°, 9°).

In the following subsections we compare the results of inverse variance beamforming with conventional beamforming, where we will focus on the following aspects: dynamic range/resultion of source maps, structure of the weighted CSM and robustness. All evaluations neglect autocorrelation measurements i.e. only off-diagonal CSM entries are considered.

3.1 Dynamic Range and Resolution

For narrowband source maps the inverse variance beamformer can improve the separation of sources. Figure 1 shows this effect for three frequencies between 3 and 4 kHz. For the inverse variance beamforming maps the peaks of each source are sharper than for the conventional beamforming maps. This enables the beamformer to identify and separate more sources from each other.

For third octave source maps we observe an improved dynamic range of the resulting source map when inverse variance beamforming is applied. The sound pressure level in regions apart from the model is much lower for the inverse variance beamformer.

For source regions with a lower SPL than the maximum SPL the inverse variance beamformer produces results with a slightly lower magnitude than the conventional beamformer. This damping effect increases as the difference of global and local maximum increases.

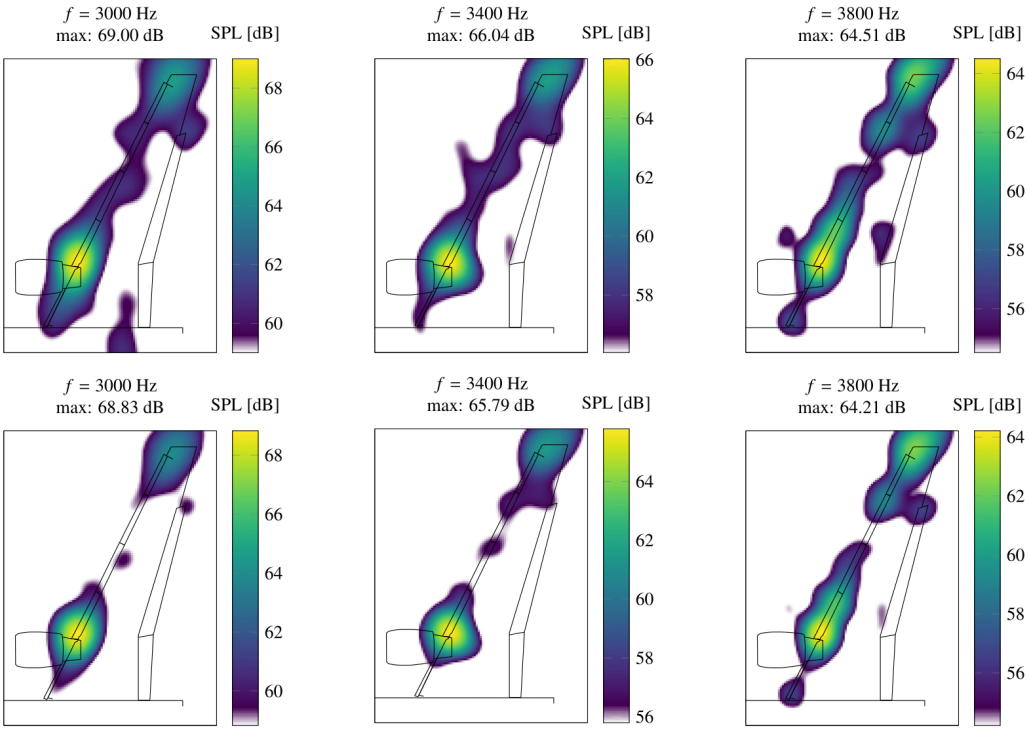

Figure 1: Narrowband source maps for conventional beamforming (upper) and inverse variance beamforming (lower). Dynamic range: $10\ dB$.

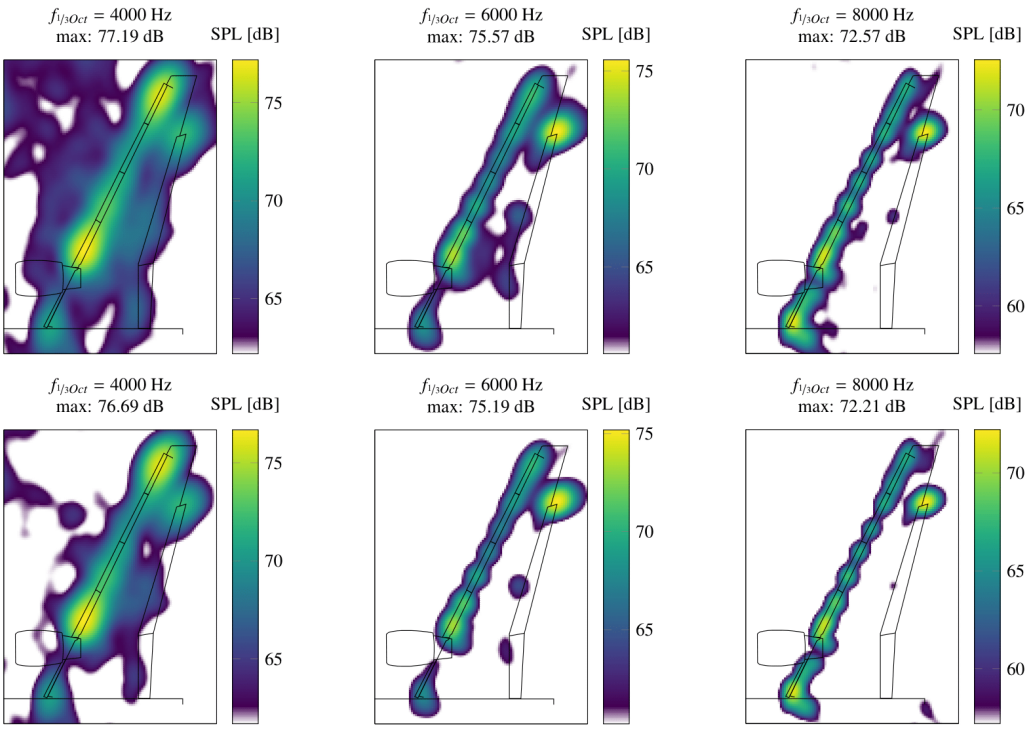

Figure 2: Third-octave band source maps for conventional beamforming (upper) and inverse variance beamforming (lower). Dynamic range: 15 *dB.*

3.2 Weighted Cross Spectral Matrix

Figure 3 shows a scatter plot of the normalized and weighted off-diagonal CSM entries at 3 and 8 kHz. There is a mild negative correlation between distance and weighted CSM entry for 3 kHz (Pearson correlation coefficient -0.057) which becomes stronger for 8 kHz (Pearson correlation coefficient -0.23).

In open test sections the turbulent shear layer induces a coherence loss between the sensor signals, which increases with the frequency and the distance [6]. As we consider a closed test section dataset, the observed damping effect may be induced by the turbulent boundary layer [7] since we observe similar scaling properties as for the coherence loss in open test sections.

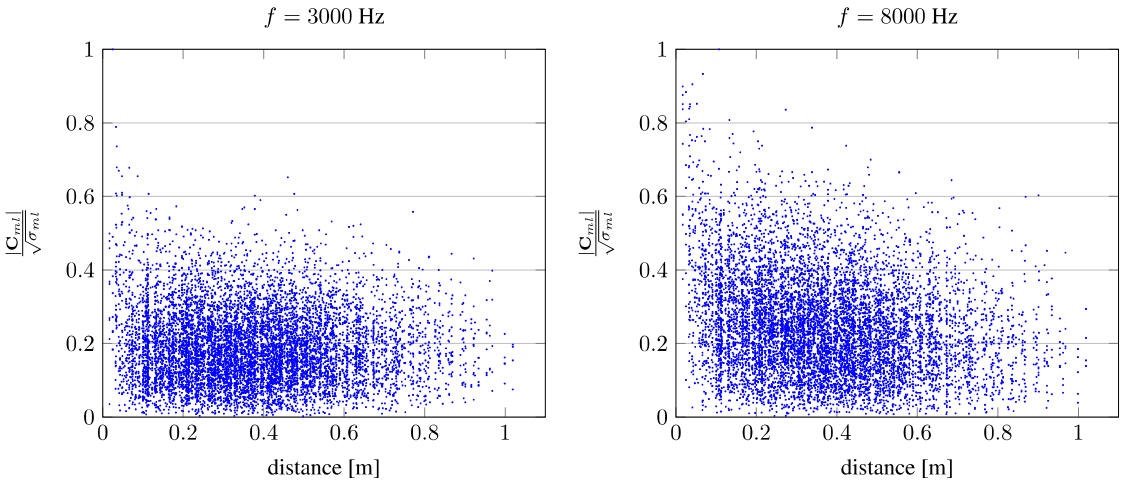

Figure 3: Normalized weighted CSM entries for 3 kHz (left) and 8 kHz (right).

3.3 Sensitivity to Defect Sensors

If a defect sensor produces an almost zero signal the corresponding cross correlations vary much less than cross correlations between correctly working sensors. Hence the variances are very low and Equation 14 indicates that cross correlations including the defect sensor get an extremely high weighting factor compared to correctly measured cross correlations. This issue makes inverse variance beamforming more sensitive to degenerated sensor signals. Conventional beamforming is known to be more robust against degenerated sensor signals (if the number of defect sensors is small). The full measurement data from the benchmark dataset includes a defect sensor whose effect on the source map will be investigated here.

The sensitivity of inverse variance beamforming to defect sensors is illustrated in Figure 4. The defect sensor has almost no effect on the resulting source map for conventional beamforming, whereas the source map for inverse variance beamforming is strongly corrupted by the degenerated sensor signal. This effect results from the extremely low variances of correlation measurements including the defect sensor. The degenerated variances are up to three orders of magnitude lower than the non degenerated ones. Removing the defect sensor from the measurement data yields a much cleaner source map for the inverse variance beamformer and the order of magnitude of the maximum SPL are now the same for both methods.

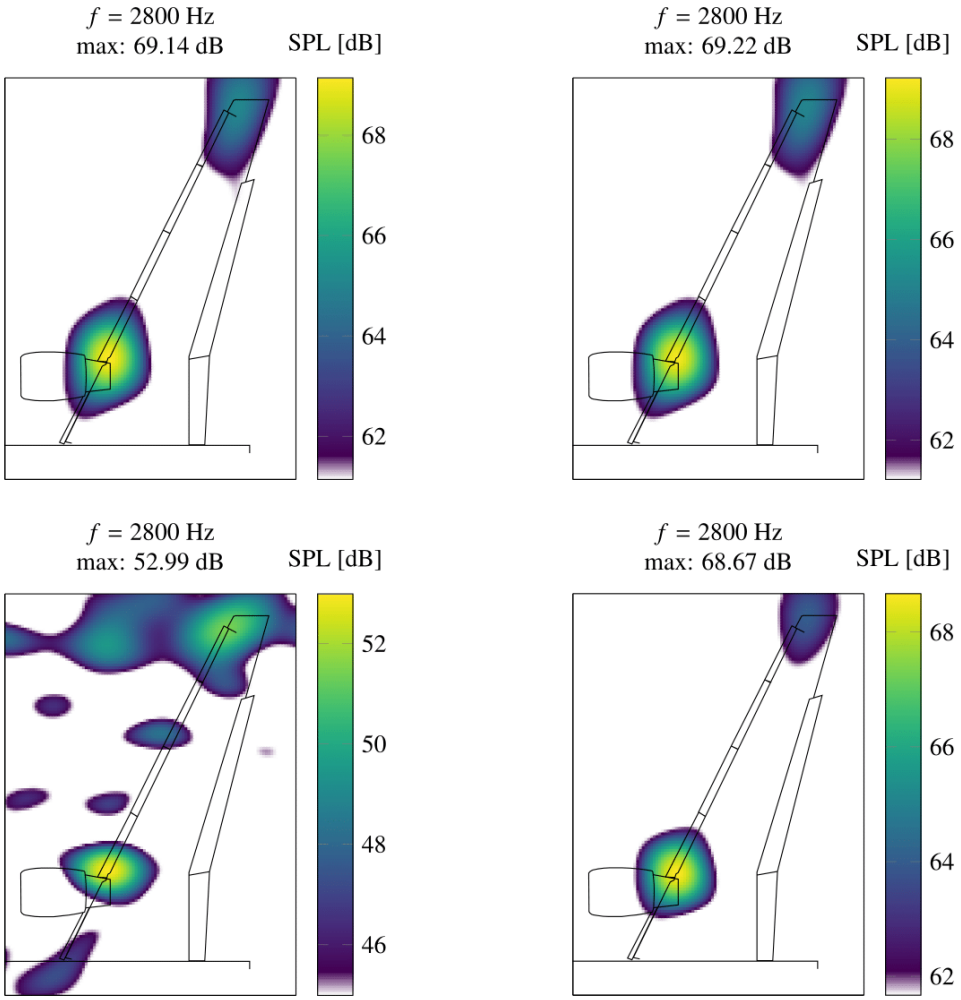

Figure 4: Illustration of sensitivity: conventional beamforming (upper) and inverse variance beamforming (lower) for measurement data including a defect sensor (left) and without defect sensor (right) .

4. CONCLUSIONS

For many aeroacoustic array imaging methods only the expected value of cross correlations is taken into account. The presented results clearly show that one can benefit from additional statistical properties (like variances) of the measurement data.

In order to guarantee a robust method, the sample variances need to be checked for outliers. For further data processing only the non degenerated variances should be taken into account.

The resulting source maps for the benchmark dataset show that the inverse variance beamformer is able to improve the resolution as well as the dynamic range. The inverse variance weighting adapts the priority of fitting a specific CSM entry. Measurements with a higher variance are considered to be less reliable and get a lower weight in the minimization target function than entries with a lower variance. The measured sample variances show that their magnitudes indeed vary strongly and thus indicate that a white noise model may be too restrictive.

The noise model of the inverse variance beamformer can be extended to correlated noise which would incorporate covariances of two CSM entries. The idea of statistical distance measures is also applicable for full inverse methods, where we solve for all focus points at once. The inverse variance weighting principle can be straightforward included in deconvolution schemes like DAMAS [8].

5. REFERENCES

References

[1] J. Billingsley and R. Kinns. The acoustic telescope. *Journal of Sound and Vibration*, 48(4):485–510, oct 1976.

[2] Pieter Sijtsma and Hermann Holthusen. Source location by phased array measurements in closed wind tunnel test sections. In *5th AIAA/CEAS Aeroacoustics Conference and Exhibit*. American Institute of Aeronautics and Astronautics, may 1999.

[3] Peter Sijtsma. Experimental techniques for identification and characterisation of noise sources. Technical report, National Aerospace Laboratory NLR, 2004.

[4] Thomas Ahlefeldt. Aeroacoustic measurements of a scaled half-model at high reynolds numbers. *AIAA Journal*, 51(12):2783–2791, dec 2013.

[5] Christopher J. Bahr, William M. Humphreys, Daniel Ernst, Thomas Ahlefeldt, Carsten Spehr, Antonio Pereira, Quentin Leclère, Christophe Picard, Ric Porteous, Danielle Moreau, Jeoffrey R. Fischer, and Con J. Doolan. A comparison of microphone phased array methods applied to the study of airframe noise in wind tunnel testing. In *23rd AIAA/CEAS Aeroacoustics Conference*. American Institute of Aeronautics and Astronautics, jun 2017.

[6] Daniel Ernst, Carsten Spehr, and Tobias Berkefeld. Decorrelation of acoustic wave propagation through the shear layer in open jet wind tunnel. In *21st AIAA/CEAS Aeroacoustics Conference*. American Institute of Aeronautics and Astronautics, jun 2015.

[7] Robert Dougherty. Turbulent decorrelation of aeroacoustic phased arrays: Lessons from atmospheric science and astronomy. In *9th AIAA/CEAS Aeroacoustics Conference and Exhibit*. American Institute of Aeronautics and Astronautics, may 2003.

[8] Thomas F. Brooks and William M. Humphreys. A deconvolution approach for the mapping of acoustic sources (DAMAS) determined from phased microphone arrays. 294(4-5):856–879.